Published for SISSA by Springer

Received: *March 25, 2026*
Revised: *July 2, 2026*
Accepted: *July 20, 2026*
Published: *September 2, 2026*

JHEP09(2026)024

A global analysis of energy-energy correlation data: determination of α_S and non-perturbative QCD parameters

Ugo Giuseppe Aglietti[a,b] **Giancarlo Ferrera**[c,d] **and Lorenzo Rossi**[c,d]

[a] *Dipartimento di Fisica, Università di Roma 'La Sapienza', Piazzale A. Moro 5, I-00185 Rome, Italy*
[b] *INFN, Sezione di Roma, Piazzale A. Moro 5, I-00185 Rome, Italy*
[c] *Dipartimento di Fisica, Università di Milano, Via G. Celoria 16, I-20133 Milan, Italy*
[d] *INFN, Sezione di Milano, Via G. Celoria 16, I-20133 Milan, Italy*

E-mail: ugo.aglietti@roma1.infn.it, giancarlo.ferrera@mi.infn.it, lorenzo.rossi3@unimi.it

Abstract: We present a comprehensive global analysis of Energy-Energy Correlation (EEC) data in electron-positron annihilation into hadrons, spanning a wide range of center-of-mass energies ($7.7\,\mathrm{GeV} \leq \sqrt{s} \leq 91.2\,\mathrm{GeV}$). In the back-to-back (two-jet) region, we resum to all orders the logarithmically-enhanced contributions up to next-to-next-to-next-to-leading logarithmic (N^{3}LL) accuracy. The resummed results are consistently matched to fixed-order calculations up to $\mathcal{O}(\alpha_S^3)$. Our resummation formalism also incorporates dominant heavy-quark mass effects and models non-perturbative power corrections by means of an analytic dispersive approach. A simultaneous fit yields an excellent description of experimental data across all energies, enabling a precise determination of the strong coupling, $\alpha_S(m_Z^2) = 0.1192 \pm 0.0028$, as well as the non-perturbative parameters, including those characterizing the Collins-Soper evolution kernel. Our analysis includes, for the first time in a global fit, datasets from the ALEPH and AMY collaborations.

Keywords: Resummation, The Strong Coupling

ArXiv ePrint: 2603.19162

https://doi.org/10.1007/JHEP09(2026)024

Contents

1 Introduction

The study of the Energy-Energy Correlation (EEC) function in high-energy electron-positron annihilation [1, 2] remains a cornerstone for testing the perturbative regime of Quantum Chromodynamics (QCD), for testing non-perturbative (NP) hadronization models, and for the precise extraction of the strong coupling constant α_S at a reference energy scale [3].

The EEC describes the distribution of the angular separation χ between pairs of energetic particles in the final state. Perturbative QCD calculations of the EEC, based on a fixed-order truncation in α_S, were made at leading order (LO, $\mathcal{O}(\alpha_S)$) in the late 1970's [1]. Subsequently, next-to-leading order (NLO, $\mathcal{O}(\alpha_S^2)$) corrections were obtained both numerically and analytically [4–7]. So far, next-to-next-to-leading order (NNLO, $\mathcal{O}(\alpha_S^3)$) corrections have been determined only numerically, through Monte Carlo integrations of the fully differential cross section for three-jet production in e^+e^- annihilation at NNLO [8–10].

In the region where the final-state hadrons are mostly emitted in two nearly back-to-back directions ($\chi \to \pi$), the fixed-order QCD perturbative expansion becomes unreliable, since its coefficients are enhanced by Sudakov logarithms, namely large double logarithms of infrared origin. The systematic resummation of these logarithmic contributions to all perturbative orders is crucial in order to obtain reliable predictions in this region. The resummation of EEC in the back-to-back region has been achieved at the next-to-leading logarithmic (NLL) accuracy in refs. [11–15] and next-to-next-to-leading logarithmic (NNLL) accuracy in refs. [8, 16, 17]. More recently, resummed predictions at the next-to-next-to-next-to-leading logarithmic accuracy (N^{3}LL) have been obtained both in the framework of Soft-Collinear Effective Theory (SCET) [18–20] and within full QCD [21].

The perturbative expansion of the EEC function also contains large (single) infrared logarithmic corrections in the forward region ($\chi \to 0^+$), where two or more energetic hadrons are produced at small angular separations (the so-called intra-jet activity). However, these

JHEP09(2026)024

effects are physically quite different from the two-jet ones, being of hard-collinear nature [21]. Finally, a realistic description of the (experimental, i.e. hadronic) EEC spectrum requires the inclusion of power-suppressed non-perturbative QCD contributions [14, 21–25].

In ref. [21], theoretical spectra, involving the resummation of Sudakov logarithms in the back-to-back region up to N^{3}LL, matched up to NNLO, have been compared with experimental data at the Z-boson resonance. The present study extends the results of ref. [21], by means of a global fit to all available datasets at different energies, and extracts both the strong coupling constant at a reference scale, as well as the non-perturbative QCD parameters. We perform the fit by consistently including data points from both the peak and the intermediate regions. This choice ensures the numerical stability of the fit and a reliable separation between perturbative and non-perturbative dynamics. Moreover, we show that the inclusion of non-perturbative power-behaved QCD effects through the analytic "dispersive approach" of ref. [21], together with a suitable energy-dependent non-perturbative evolution, provides an excellent description of the data across all energies.

We believe that the use of an analytic dispersive model for non-perturbative power corrections is a significant advantage of our method; unlike methods which extract hadronization corrections by means of general-purpose Monte-Carlo event generators (which may introduce tune-dependent biases and unclear theoretical uncertainties), our approach treats non-perturbative effects via an analytic parameterization, which is fitted simultaneously with α_S. This ensures better control over both QCD perturbative and non-perturbative effects.

In the end, we obtain a precise determination of $\alpha_S(m_Z^2) = 0.1192 \pm 0.0028$, which turns out to be fully consistent with the current global average [26]. Moreover, by analyzing EEC spectra at different energies simultaneously, we disentangle the energy-dependent components of the non-perturbative form factor, enabling a novel extraction of the Collins-Soper kernel.

A novel aspect of our global analysis is the inclusion of very recent, high-precision measurements of the EEC from the Electron-Positron Alliance collaboration [27, 28], based on a reanalysis of archived ALEPH data available at $\sqrt{s} = 91.2\,\mathrm{GeV}$. Furthermore, we extend the experimental coverage of our global analysis by including previously unused datasets from the AMY collaboration at $\sqrt{s} = 58.0\,\mathrm{GeV}$ allowing for a more robust test of the QCD evolution predicted by the Collins-Soper kernel. We will show that our theoretical framework successfully achieves an excellent description of these precise measurements alongside the legacy data.

The structure of the paper is as follows. In section 2 we present a concise review of the theoretical framework. Section 3 describes the datasets, the treatment of the uncertainties and the methodology used for the parameter extraction. The results, including a brief discussion of heavy quark mass effects, are presented in section 4. Our conclusions are summarized in section 5.

2 Formalism

The Energy-Energy Correlation (EEC) function is defined as:

$$\frac{d\Sigma}{d\cos\chi} = \sum_{n=2}^{\infty} \sum_{i,j=1}^{n} \int \frac{E_i}{Q} \frac{E_j}{Q} \, \delta(\cos\chi - \cos\theta_{ij}) \, d\sigma^{(n)}_{e^+e^- \to h_i h_j + X} \,, \tag{2.1}$$

where the sum runs over all pairs of final-state particles (i, j), with energies E_i and E_j, for events containing $n \geq 2$ hadrons. The variable θ_{ij} denotes the relative angle between their spatial momenta, and the hard scale $Q = \sqrt{s}$ is identified with the center-of-mass energy of the colliding e^+e^- pair.

It is useful to express the EEC in terms of the dimensionless unitary variable

$$z \equiv \frac{1 - \cos\chi}{2} = \sin^2 \frac{\chi}{2} \,. \tag{2.2}$$

Experimental measurements are typically presented after normalization to the total cross section σ_{tot}, defined as

$$\sigma_{\text{tot}} = \int_{-1}^{+1} \frac{d\Sigma}{d\cos\chi} d\cos\chi = \int_0^1 \frac{d\Sigma}{dz} dz = \int \left(\sum_{i=1}^{n} \frac{E_i}{Q} \right)^2 d\sigma = \int d\sigma \,. \tag{2.3}$$

2.1 Resummation in the two-jet region

In the back-to-back region ($z \to 1^-$ or $\chi \to \pi$), in which all energetic hadrons in the final states are collimated in two opposite directions, the convergence of the standard fixed-order perturbative QCD expansion is spoiled, since its coefficients are enhanced by large double logarithms of infrared (soft and collinear) origin. To obtain reliable perturbative predictions, these so-called Sudakov logarithms have to be resummed to all orders in α_S. For this purpose, the normalized EEC distribution is conveniently decomposed as

$$\frac{1}{\sigma_{\text{tot}}} \frac{d\Sigma}{dz} = \frac{1}{\sigma_{\text{tot}}} \frac{d\Sigma_{(res.)}}{dz} + \frac{1}{\sigma_{\text{tot}}} \frac{d\Sigma_{(fin.)}}{dz} \,, \tag{2.4}$$

where the first term on the r.h.s., the *resummed* term, factorizes and resums to all orders the logarithmically enhanced contributions (it includes also the $\delta(1-z)$ terms), while the second term denotes the *finite* (i.e. free from large infrared logarithms) remainder function and is computed at fixed order.

In order to consistently take into account the kinematic constraint of transverse momentum conservation in multiple parton emissions, the resummation is made in the impact-parameter b-space [11, 12, 14], where b is conjugate to the variable $Q\sqrt{1-z}$. In b-space, the back-to-back limit $1 - z \ll 1$ corresponds to the region $bQ \gg 1$ and the large Sudakov logarithms are of the form $\alpha_S^n \ln^k(Q^2b^2)$, with $1 \leq k \leq 2n$. After the resummation procedure has been carried out, the resummed part of the distribution in physical space is recovered by means of an inverse Fourier-Bessel transform:

$$\frac{1}{\sigma_{\text{tot}}} \frac{d\Sigma_{(res.)}}{dz} = \frac{1}{2} H(\alpha_S) \int_0^\infty d(Qb) \frac{Qb}{2} J_0(\sqrt{1-z}\, Qb)\, S(b, Q) \,, \tag{2.5}$$

where $J_0(x)$ denotes the Bessel function of the first kind of zero order.

As shown in eq. (2.5), the resummed component of the EEC distribution factorizes into a hard function $H(\alpha_S)$ and a Sudakov form factor $S(b, Q)$. The hard function $H(\alpha_S)$, which encodes hard-virtual corrections and is independent of b, admits a standard perturbative expansion:

$$H(\alpha_S) = 1 + \sum_{n=1}^{\infty} \left(\frac{\alpha_S}{\pi} \right)^n H_n \,, \tag{2.6}$$

where the QCD coupling $\alpha_S \equiv \alpha_S(\mu_R^2)$ is evaluated at the renormalization scale $\mu_R = \mathcal{O}(Q)$.

The Sudakov form factor $S(b,Q)$ resums, to all orders in the conjugate b-space, the large Sudakov logarithms and can be expressed in the following exponential form [11, 14, 29]:

$$S(b,Q) = \exp\left\{ -\int_{b_0^2/b^2}^{\mu_Q^2} \frac{dq^2}{q^2} \left[A\Big(\alpha_S(q^2)\Big) \ln\frac{Q^2}{q^2} + B\Big(\alpha_S(q^2)\Big) \right] \right\}, \tag{2.7}$$

where $b_0 \equiv 2\exp(-\gamma_E) \simeq 1.123$ ($\gamma_E = 0.5772\cdots$ is the Euler-Mascheroni number) is a kinematic coefficient and μ_Q denotes the resummation scale which takes into account the arbitrariness associated in the resummation procedure [29]. The central (reference) values of μ_R and μ_Q have to be chosen of the order of the hard scale Q. Variations around the central values are typically made to estimate the corresponding perturbative uncertainties in the renormalization and resummation procedure. The perturbative expansion of the double-logarithmic and single-logarithmic functions $A(\alpha_S)$ and $B(\alpha_S)$ in eq. (2.7) reads

$$A(\alpha_S) = \sum_{n=1}^{\infty} \left(\frac{\alpha_S}{\pi}\right)^n A_n\,, \tag{2.8}$$

$$B(\alpha_S) = \sum_{n=1}^{\infty} \left(\frac{\alpha_S}{\pi}\right)^n B_n\,. \tag{2.9}$$

After analytical integration in eq. (2.7), the Sudakov form factor can be explicitly written in the form [16, 21, 30]:

$$S(b,Q) = \exp\left\{ \widetilde{L}\, g_1(\lambda) + g_2(\lambda) + \frac{\alpha_S}{\pi} g_3(\lambda) + \left(\frac{\alpha_S}{\pi}\right)^2 g_4(\lambda) + \sum_{n=3}^{+\infty} \left(\frac{\alpha_S}{\pi}\right)^n g_{n+2}(\lambda) \right\}, \tag{2.10}$$

with

$$\lambda \equiv \frac{\alpha_S(\mu_R^2)}{\pi} \beta_0 \widetilde{L} \quad \text{and} \quad \widetilde{L} = \ln\left(\frac{\mu_Q^2 b^2}{b_0^2} + 1\right), \tag{2.11}$$

where β_0 is the first-order coefficient of the QCD β-function. The use of the logarithmic variable $\widetilde{L}$ (rather than the usual $L \equiv \ln(\mu_Q^2 b^2/b_0^2)$) ensures the correct unitarity constraint [29] and prevents spurious unphysical divergences in the limit $b \to 0^+$. The explicit analytic expressions of the functions $g_n(\lambda)$ up to next-to-next-to-next-to-leading logarithmic (N^{3}LL), i.e. up to $g_4(\lambda)$ included, together with the numerical values of the corresponding coefficients, can be found in ref. [21].

We observe that the functions $g_n(\lambda)$ depend explicitly both on the unphysical renormalization (μ_R) and resummation (μ_Q) scales. This artificial dependence reduces by increasing the perturbative accuracy of the calculation and formally vanishes by including all orders. We emphasize that, due to the singularity of the QCD coupling at the scale Λ_{QCD} (a simple pole at lowest order), the functions $g_n(\lambda)$ are singular at the point $\lambda = 1$, which actually corresponds to the value of the impact parameter $b_L = b_0/Q \exp[\pi/(2\beta_0\alpha_S)] \simeq 1/\Lambda_{QCD}$. Therefore, in order to evaluate the integral in eq. (2.5), a non-perturbative prescription is needed. In this work, we use the so-called $b_\star$ prescription [12, 13, 31, 32], which regularizes the integral by freezing the value of the impact parameter b before it reaches the Landau singularity at b_L. This is achieved by introducing a parameter $b_{\max} < b_L$ and replacing b as

$$b \mapsto b_\star \equiv \frac{b}{\sqrt{1 + b^2/b_{\max}^2}}\,. \tag{2.12}$$

JHEP09(2026)024

Although this prescription guarantees that the variable $b_\star$ saturates at $b_{\max}$ at large values of b, then avoiding the Landau singularity, it also introduces a nonphysical dependence on $b_{\max}$ in the form of spurious power corrections that must be compensated for (we will comment below).

The finite component of the distribution in eq. (2.4) is a process-dependent function, which is obtained from the fixed-order result by subtracting the perturbative expansion of the resummed contribution, truncated at the same perturbative order:

$$\frac{1}{\sigma_{\rm tot}}\frac{d\Sigma_{(fin.)}}{dz} = \frac{1}{\sigma_{\rm tot}}\frac{d\Sigma_{(f.o.)}}{dz} - \frac{1}{\sigma_{\rm tot}}\frac{d\Sigma_{(res.)}}{dz}\bigg|_{\rm f.o.} . \tag{2.13}$$

For $z > 0$, the finite remainder admits a standard perturbative expansion

$$\frac{1}{\sigma_{\rm tot}}\frac{d\Sigma_{(fin.)}}{dz} = \frac{\alpha_S}{\pi}\,\widetilde{\mathcal{A}}_{(fin.)}(z) + \left(\frac{\alpha_S}{\pi}\right)^2\widetilde{\mathcal{B}}_{(fin.)}(z) + \left(\frac{\alpha_S}{\pi}\right)^3\widetilde{\mathcal{C}}_{(fin.)}(z) + \mathcal{O}(\alpha_S^4)\,, \tag{2.14}$$

where the coefficients of the powers of α_S/π have been explicitly given in [21] up to the next-to-next-to-leading order (NNLO), i.e. $\mathcal{O}(\alpha_S^3)$.

2.2 Non-perturbative model

We incorporate non-perturbative effects in our theoretical description of the EEC, by multiplying the Sudakov form factor $S(b, Q)$ by the following NP form factor

$$S_{NP}\left(b, \frac{Q}{Q_0}\right) = \exp\left[-f(b) - g_K(b)\,\ln\left(\frac{Q^2}{Q_0^2}\right)\right] . \tag{2.15}$$

The function $f(b)$ parameterizes the non-perturbative effects at very large values of b ($b \gtrsim 1\ \mathrm{GeV}^{-1}$) at a reference energy scale Q_0, while the function $g_K(b)$ encodes the NP evolution from Q_0 to Q and is thus the NP component of the so-called Collins-Soper evolution kernel [12, 13, 31, 32]. By requiring NP effects to vanish in the perturbative region (i.e. at small b), we impose $S_{NP}(b = 0, Q/Q_0) = 1$ which implies $f(0) = g_K(0) = 0$. In this work, we set $Q_0 = 1\,\mathrm{GeV}$ and use the following parameterization

$$f(b) = f_1\, b + f_2\, b^2\,, \tag{2.16}$$

$$g_K(b) = g_0\left\{1 - \exp\Big[-\frac{C_F\,\alpha_S\,(b_0^2/b_\star^2)}{\pi g_0}\,\frac{b^2}{b_{\max}^2}\Big]\right\}\,; \tag{2.17}$$

where g_0, f_1 and f_2 are NP parameters to be extracted from the experimental data. The functional form in eq. (2.16), with a linear and a quadratic term in b, is the same dictated by the Dokshitzer-Marchesini-Webber (DMW) dispersive model [24, 25] and successfully used in ref. [21] to describe the data at the Z-boson resonance. The functional form of $g_K(b)$ in eq. (2.17) has been proposed in ref. [33] and has been successfully used in global analysis of the Drell-Yan transverse-momentum distribution at various center-of-mass energies [34] but also in a precise determination of α_S in refs. [35, 36]. It has been chosen in order to cancel the leading $\mathcal{O}(b^2/b_{\max}^2)$ dependence of the perturbative form factor $S(Q, b)$ from $b_{\max}$, leaving a residual $\mathcal{O}(b^4/b_{\max}^4)$ dependence. In this work we use $b_{\max} = b_0 = 2\exp\{-\gamma_E\} \simeq 1.123\,\mathrm{GeV}^{-1}$.

JHEP09(2026)024

2.3 Heavy-quark mass effects

In ref. [37], heavy-quark contributions to the Sudakov form factor of the EEC distribution were computed. In this work, we investigate the impact of these effects on our analysis. In particular, by including finite-mass effects only for the bottom quark, we rewrite the form factor $S(b,Q)$ entering eq. (2.5) as [37]:

$$\begin{aligned} S(b,Q) \mapsto S(b,Q)\,\theta(b_{\rm cr}-b) + \Bigg[& \frac{c_b(Q^2)}{\sum_f c_f(Q^2)} S(b_{\rm cr},Q) S_m(b,Q)|_{n_f=4} \\ & + \left(1-\frac{c_b(Q^2)}{\sum_f c_f(Q^2)}\right) S(b,Q)\Big|_{n_f=4}\Bigg]\,\theta(b-b_{\rm cr}), \end{aligned} \tag{2.18}$$

where $b_{\rm cr} \equiv b_0/m_b$ is the critical length below which the effects of the bottom-quark mass m_b are neglected and $S_m(b,Q)$ is the massive Sudakov form factor, whose explicit expression can be found in [37]. The subscript $n_f = 4$ denotes the terms in which the number of active quark flavors n_f has been reduced from five to four, in order to remove the contribution from a massive (real or virtual) heavy quark pair. The sum in eq. (2.18) runs over all active quark flavors, $f = u, d, c, s, b$, and c_f is the electroweak coefficient related to quark flavor f, given, in the massless case, by [38]

$$c_f(Q^2) = Q_f^2 - 2V_e Q_f V_f\,\chi_1(Q^2) + (V_e^2+A_e^2)\,(V_f^2+A_f^2)\,\chi_2(Q^2), \qquad f = u,d,s,c\,. \tag{2.19}$$

In the bottom-quark case, by including leading mass effects:

$$\begin{aligned} c_b(Q^2) = \Bigg\{ & \left[Q_b^2 - 2V_e Q_b V_b\,\chi_1(Q^2) + \left(V_e^2+A_e^2\right) V_b^2\,\chi_2(Q^2)\right]\beta\frac{3-\beta^2}{2}\left[1+(c_1-1)\,\frac{\alpha_S}{\pi}\right] \\ & + \left(V_e^2+A_e^2\right) A_b^2\,\chi_2(Q^2)\beta^3\left[1+(d_1-1)\,\frac{\alpha_S}{\pi}\right]\Bigg\}\,\theta(Q-2m_b). \end{aligned} \tag{2.20}$$

$\theta(x) \equiv 1$ for $x > 0$ and zero otherwise is the Heaviside step function and β is the (ordinary) velocity of the bottom quark,

$$\beta = \sqrt{1-\frac{4m_b^2}{Q^2}}, \tag{2.21}$$

with m_b the on-shell bottom-quark mass. The coefficients c_1 and d_1 are the $\mathcal{O}(\alpha_S)$ polar-vector and axial-vector corrections to the total cross section of $e^+e^- \to b\bar{b}$ in the massive case, respectively:

$$\begin{aligned} c_1 &= 1 + 12\,\epsilon + \mathcal{O}(\epsilon^2); \\ d_1 &= 1 - 22\,\epsilon + \mathcal{O}(\epsilon^2); \end{aligned} \tag{2.22}$$

where:

$$\epsilon \equiv \frac{\overline{m}_b^2(Q^2)}{Q^2} \ll 1. \tag{2.23}$$

JHEP09(2026)024

$\overline{m}_b(Q^2)$ is the $\overline{\text{MS}}$ (running) bottom-quark mass at the renormalization scale $\mu = Q$. The functions χ_i, $i = 1, 2$, involving the Z^0-exchange diagram, explicitly read:

$$\chi_1(Q^2) = \frac{1}{4\sin^2\theta_W \cos^2\theta_W} \frac{Q^2(Q^2 - m_Z^2)}{(Q^2 - m_Z^2)^2 + m_Z^2\Gamma_Z^2}\,, \tag{2.24}$$

$$\chi_2(Q^2) = \frac{1}{16\sin^4\theta_W \cos^4\theta_W} \frac{Q^4}{(Q^2 - m_Z^2)^2 + m_Z^2\Gamma_Z^2}\,, \tag{2.25}$$

where the constants Q_f, V_f and A_f represent the electric, vector, and axial charges of flavor f respectively; V_e and A_e are the vector and axial charges of the electron; θ_W is the weak mixing angle; Γ_Z and m_Z are the width and mass of the Z boson. We use the following numerical values: $\Gamma_Z = 2.4950\,\text{GeV}$, $m_Z = 91.1876\,\text{GeV}$, $\sin^2\theta_W = 0.23121$, $\overline{m}_b(\overline{m}_b^2) = 4.2\,\text{GeV}$ [26].

3 Data and fitting procedure

The experimental data set used in this analysis includes all available measurements of the EEC function, including the recent reanalysis of the ALEPH Coll. [27, 28] at $\sqrt{s} = 91.2\,\text{GeV}$ and the analysis of the AMY Coll. [39] at $\sqrt{s} = 58.0\,\text{GeV}$. Notably, these specific datasets are included here for the first time in a global EEC analysis, providing unique constraints on the energy evolution of the distribution. We find that our theoretical framework provides an excellent description of these additional datasets, with a χ^2 per degree of freedom of the order of unity.

Let us remark that the ALEPH analysis includes only charged final-state particles and therefore differs from the fully inclusive EEC observable. In section 4 we discuss the origin of this difference and show that it is numerically negligible. As a further check, we perform a fit without the ALEPH dataset and show that the extracted parameters do not significantly change. Finally, we show that our theoretical framework provides an excellent description of the ALEPH data, with a χ^2 per degree of freedom of order unity, both when the dataset is directly included in the fit and when a postdiction is performed to assess the level of agreement with the other measurements.

Following ref. [21], in our numerical analysis we perform the fit by consistently including data points from both the peak and the intermediate regions. This strategy ensures a reliable extraction of the non-perturbative parameters, as well as a robust determination of the strong coupling constant. We therefore restrict the analysis to the region of intermediate and large values of the χ kinematic variable:[1]

$$1.8 \leq \chi \leq \pi\,. \tag{3.1}$$

In total, 691 data points are included in the fit, which decrease to 610 if the ALEPH dataset is excluded. The relevant information for each dataset is summarized in table 1.

As pointed out in refs. [17, 54], a key aspect of a global analysis of EEC data is the treatment of experimental uncertainties. Here we follow the approach adopted in ref. [17]. In particular, for datasets where statistical and systematic uncertainties are provided separately, we treat them consistently. For datasets where only partial information on systematic

[1] We have verified that our results are stable under small variations of this range.

Experiment	$N_{\rm dat}$	$\sqrt{s}$ [GeV]	Ref.
OPAL (1992)	43	91.3	[40]
OPAL (1993)	77	91.2	[41]
DELPHI (1992)	21	91.2	[42]
DELPHI (1993)	21	91.2	[43]
L3	15	91.2	[44]
SLD	21	91.2	[45]
ALEPH	81	91.2	[27, 28]
TOPAZ	21 21	59.5 53.3	[46]
AMY	43	58.0	[39]
TASSO	21 21 21 21	43.5 34.8 22.0 14.0	[47]
PLUTO	13	34.6	[48]
PLUTO	8 8 8 8 8 8 8 6	30.8 27.6 22 17 13 12 9.4 7.7	[49]
JADE	21 21 21	34.0 22.0 14.0	[50]
CELLO	21 21	34.0 22.0	[51]
MARKII Run I	21	29.0	[52]
MARKII Run II	21	29.0	[52]
MAC	21	29.0	[53]
Total	691		

Table 1. Experimental data sets included in this analysis. Each row contains the name of the collaboration, the number of data points ($N_{\rm dat}$) included, the center-of-mass energy $\sqrt{s}$ and the reference.

uncertainties is available, we estimate them following the procedure of ref. [17]. For all remaining datasets, the published combined uncertainties are treated as purely statistical.

Another important aspect discussed in ref. [17] is the presence of correlations between different bins within the same experiment. Since correlation matrices are not available for all datasets, we assess their impact by considering two scenarios. In the first, no correlations are included, reflecting the information directly available. In the second, following ref. [17], we assume a correlation coefficient $\rho = 0.5$ between adjacent bins of the same experiment, for both statistical and systematic uncertainties. The associated uncertainty is then estimated from the spread of the fitted parameters obtained in the two scenarios. We perform a fit to determine the optimal values of $\alpha_S(m_Z^2)$ and of the non-perturbative parameters f_1, f_2, and g_0 entering eq. (2.15). The best-fit parameters are obtained by minimizing the following χ^2 function:

$$\chi^2 = \sum_{d \in \text{datasets}} \chi_d^2 = \sum_{d \in \text{datasets}} \left(\vec{D}_d - \vec{P}_d\right)^T V_d^{-1} \left(\vec{D}_d - \vec{P}_d\right) , \tag{3.2}$$

where the index d runs over all available datasets. The vector $\vec{D}_d$ denotes the data points of the d-th dataset, V_d is the corresponding covariance matrix, and $\vec{P}_d$ represents the theoretical predictions for that dataset.

In order to obtain a reliable estimate of the uncertainties on $\alpha_S(m_Z^2)$ and on the non-perturbative parameters arising from experimental uncertainties, we employ the *bootstrap* method. This method, originally introduced for collinear PDF fits [55, 56], consists in generating replicas of the dataset by adding Gaussian fluctuations according to the experimental uncertainties and fitting each replica independently. We generate 1000 replicas, obtaining 1000 sets of best-fit parameters. By construction, their mean values coincide with the central values obtained from the fit to the original dataset, while their standard deviations provide the corresponding uncertainties at the 68% confidence level. Further details can be found in refs. [55, 56]. To estimate the size of missing higher-order contributions and the associated perturbative uncertainties, we consider conventional variations of the auxiliary scales μ_R and μ_Q. In particular, we perform fits by varying μ_R and μ_Q independently within the range

$$\frac{Q}{2} \leq \{\mu_R, \mu_Q\} \leq 2Q \, , \tag{3.3}$$

subject to the constraint

$$\frac{1}{2} \leq \frac{\mu_R}{\mu_Q} \leq 2 \, . \tag{3.4}$$

At the end of the analysis, the fitted parameters are assigned three different sources of uncertainty: experimental, correlation-related, and perturbative. The total uncertainty for α_S (and analogously for the non-perturbative parameters) is expressed as

$$\delta\alpha_S = \sqrt{(\delta\alpha_S^{\text{exp}})^2 + (\delta\alpha_S^{\text{corr}})^2 + (\delta\alpha_S^{\text{th}})^2} \, , \tag{3.5}$$

where $\delta\alpha_S^{\text{exp}}$ represents the uncertainty due to experimental fluctuations, $\delta\alpha_S^{\text{corr}}$ accounts for the modeling of bin-to-bin correlations, and $\delta\alpha_S^{\text{th}}$ denotes the perturbative uncertainty estimated from the envelope of the fits obtained under scale variations.

JHEP09(2026)024

4 Results

In this section, we present the results obtained by applying the formalism described in the previous sections at N^{3}LL+NNLO accuracy.

In general, we find an excellent description of the data, as indicated by the value $\chi^2/N_{\text{d.o.f.}} = 1.2$, obtained from the fit to the unfluctuated (central) dataset without including any correlations (i.e. $\rho = 0$). We have also investigated the impact of bin-to-bin correlations by performing an alternative fit that assumes a correlation coefficient $\rho = 0.5$ between adjacent bins within the same dataset, as described in section 3. In this case, we obtain $\chi^2/N_{\text{d.o.f.}} = 1.4$, which is compatible with the uncorrelated result. This indicates that our conclusions are stable under reasonable assumptions about the correlation structure. The variations in the fitted parameters are included in the total uncertainty, as described in the previous section, and are reported in table 2.

In figure 1 we compare the theoretical predictions obtained from the global fit with experimental data from LEP (CERN) and SLC (SLAC) [40–45], corresponding to measurements at the Z-boson mass. The blue uncertainty bands represent the estimated theoretical uncertainties, evaluated through standard scale variations (see eqs. (3.3) and (3.4)). The experimental data are well described, within uncertainties, over the entire selected angular range. This provides clear evidence that the formalism described in section 2, supplemented by an analytic non-perturbative model, is able to accurately describe the data. Moreover, the uncertainty bands are comparable to those obtained from a fit using only Z-pole data [21]. This indicates the absence of significant tensions between measurements at the Z^0 peak and at lower energies.

One of the main novelties of this work is the inclusion of the recent reanalysis of archived data from the ALEPH Coll. at the Z-boson resonance [27, 28].[2] In figure 2, we compare our theoretical predictions with these recent high-precision measurements. The EEC distribution is shown both as a function of χ and as a function of z on logarithmic scales. By going from the variable χ to the variable z, the back-to-back region, which is our primary concern, is strongly compressed, and the peak disappears. Our N^{3}LL+NNLO predictions, supplemented by the analytic dispersive model, achieve a very good description of this novel dataset across the entire available spectrum. This remarkable agreement, also in the case of smaller experimental uncertainties, further confirms the robustness of our theoretical framework.

The ALEPH dataset differs from the other measurements included in this analysis in that it is based on charged final-state particles only, rather than on the fully inclusive hadronic final state. Strictly speaking, the theoretical framework described in section 2 computes the EEC summed over all final-state hadrons. However, as we discuss below, the difference between the charged-particle EEC and the fully inclusive EEC is numerically negligible in the kinematic region relevant for our fit.

The charged and the inclusive EEC are related by

$$\frac{1}{\sigma_{\text{tot}}^{ch}}\frac{d\Sigma^{\text{ch}}}{d\cos\chi} = \frac{1}{\sigma_{\text{tot}}}\frac{d\Sigma}{d\cos\chi}\cdot\left[1+\varepsilon(\chi)\right], \tag{4.1}$$

[2] It is worth emphasizing that the experimental data from the ALEPH collaboration have been accurately self-extracted from the original publications, as the corresponding numerical tables are not available in public databases.

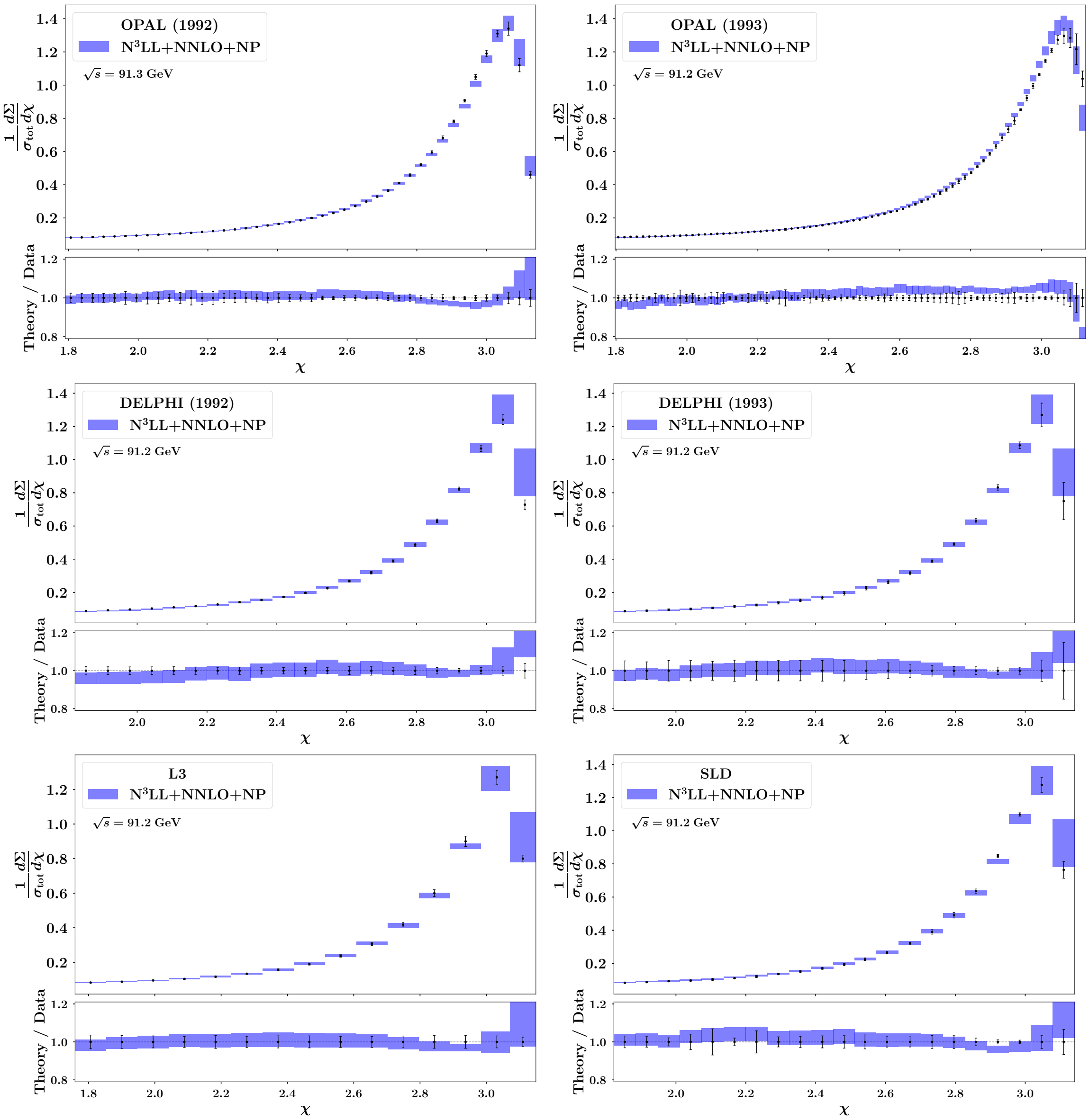

Figure 1. Comparison between experimental data and theoretical predictions (blue bands) for the EEC distribution at the Z-boson resonance from OPAL Coll. (top left and top right), DELPHI Coll. (middle left and right), L3 Coll. (bottom left) and SLD Coll. (bottom right). The uncertainty bands represent the theoretical uncertainties estimated through scale variations. The lower panels show the ratio of the theoretical results to the experimental data.

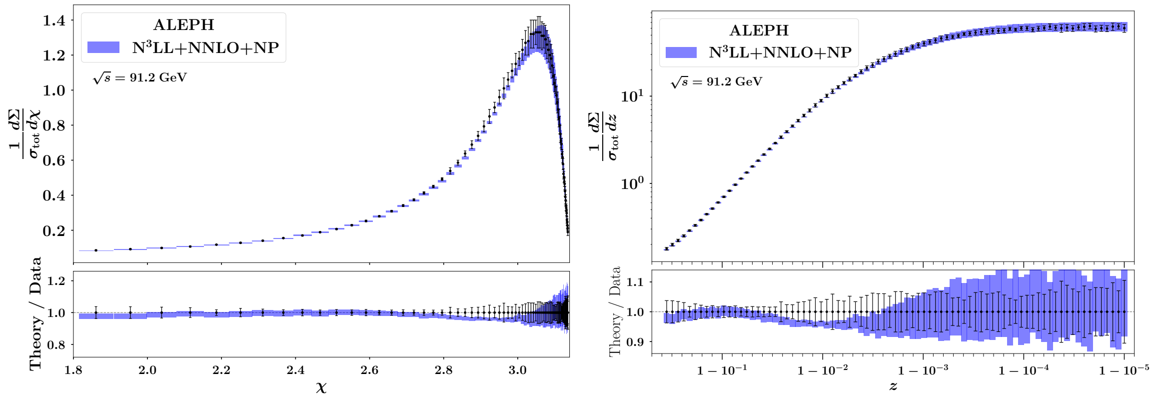

Figure 2. Comparison between the recent reanalysis of archived experimental data from ALEPH Coll. at $\sqrt{s} = 91.2\,\text{GeV}$ and our theoretical predictions (blue bands). The EEC distribution is shown as a function of χ (left panel) and as a function of z on logarithmic scales (right panel), the latter emphasizing the back-to-back region where resummation and non-perturbative effects are most prominent. The uncertainty bands represent the theoretical uncertainties estimated through scale variations. The lower panels show the ratio of the theoretical results to the experimental data. The superscript *ch.* indicates that the ALEPH analysis is based on charged final-state particles only, rather than on the fully inclusive hadronic final state.

where $\sigma_{\rm tot}^{\rm ch}$ denotes the charged-weighted total cross section, defined as

$$\sigma_{\rm tot}^{\rm ch} = \int d\sigma \left(\sum_{i\in \rm ch} \frac{E_i}{Q} \right)^2 \tag{4.2}$$

and $\varepsilon(\chi)$ parameterizes the residual χ-dependent corrections.

The subleading correction $\varepsilon(\chi)$ receives contributions from two distinct non perturbative sources. The first is associated with event-by-event fluctuations of the charged energy fraction, $r \equiv \sum_{i\in \rm ch} E_i/Q$, around its mean value. The second arises from the χ-dependent isospin composition of the hadronic final state, which is governed by hadronization dynamics. The fluctuation contribution is suppressed by the large final-state multiplicity at LEP energies, where $\langle n_{\rm ch}\rangle \simeq 21$ at $\sqrt{s} = M_Z$. The χ-dependent isospin correction is further suppressed in the back-to-back region, where the two-jet configuration is dominated by a single quark flavour in each hemisphere and the charged-to-neutral energy ratio approaches a constant.

We have verified this picture quantitatively by means of PYTHIA 8.3 [57] simulations of $e^+e^- \to$ hadrons at $\sqrt{s} = M_Z$ including NP hadronization effects. The ratio $\frac{1}{\sigma_{\rm tot}^{ch}}\frac{d\Sigma^{\rm ch}}{d\cos\chi} / \frac{1}{\sigma_{\rm tot}}\frac{d\Sigma}{d\cos\chi}$ is found to be flat in χ at 1% level across the entire fit range $\chi \in [1.8, 3.0]$, increasing to few percent level for $\chi > 3.0$. This confirms that the shape distortion induced by the charged-only restriction is well below the theoretical and experimental uncertainties of our analysis. As a further cross-check, we note that our theoretical predictions provide an excellent description of the ALEPH data, with a χ^2 per degree of freedom of order unity ($\chi^2/N_{\rm d.o.f.} = 0.94$), and that no tension is observed between the ALEPH dataset and the other measurements included in the fit. This provides direct empirical evidence that the effect of using charged particles only is negligible at the level of precision of the present analysis.

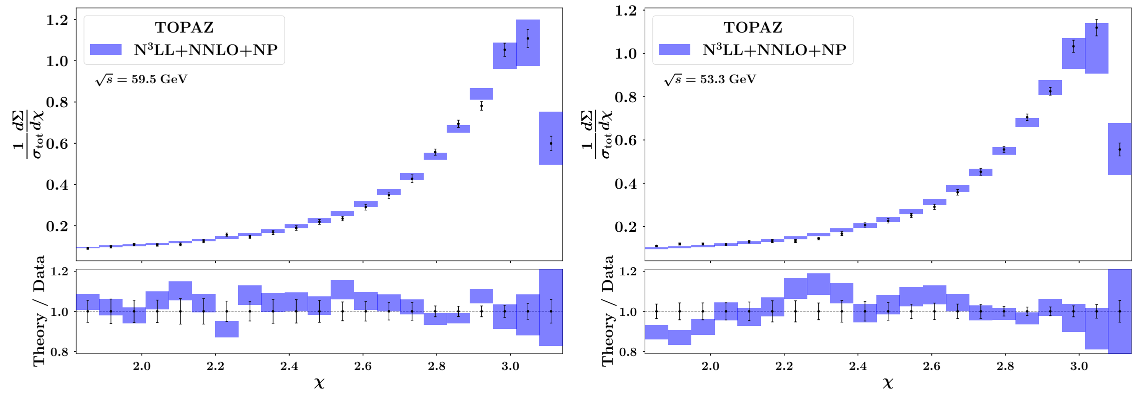

Figure 3. Comparison between experimental data and theoretical predictions (blue bands) for the EEC distribution from TOPAZ Coll. at $\sqrt{s} = 59.5\,\text{GeV}$ (left) and $\sqrt{s} = 53.3\,\text{GeV}$ (right). The uncertainty bands represent the theoretical uncertainties estimated through scale variations. The lower panels show the ratio of the theoretical results to the experimental data.

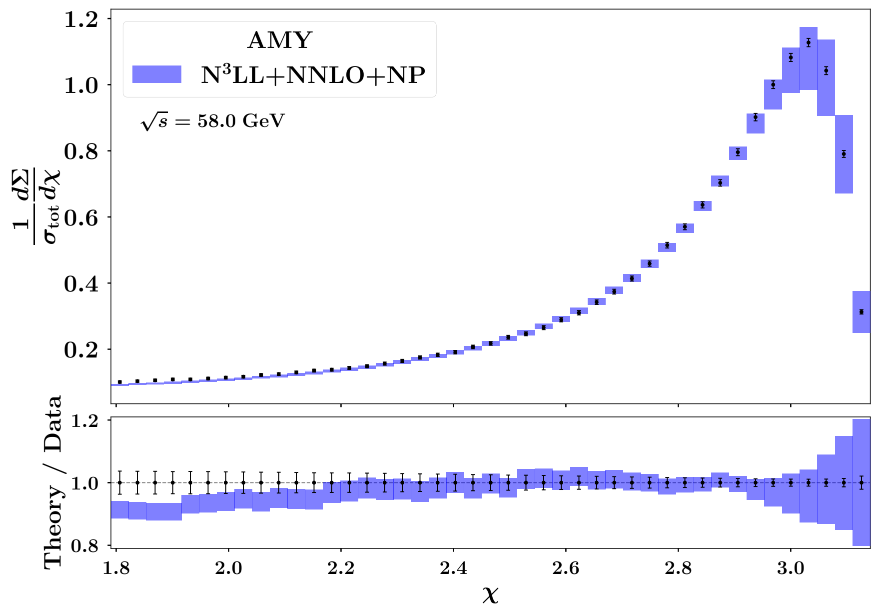

Figure 4. Comparison between experimental data and theoretical predictions (blue bands) for the EEC distribution from AMY Coll. at $\sqrt{s} = 58.0\,\text{GeV}$. The uncertainty bands represent the theoretical uncertainties estimated through scale variations. The lower panels show the ratio of the theoretical results to the experimental data.

We now consider data at center-of-mass energies below the Z-boson resonance. In figures 3 and 4 we compare our theoretical predictions with experimental data from the TOPAZ Collaboration [46] at $\sqrt{s} = 59.5\,\text{GeV}$ (left panel) and $\sqrt{s} = 53.3\,\text{GeV}$ (right panel), and from the AMY Collaboration [39] at $\sqrt{s} = 58.0\,\text{GeV}$ collected at the TRISTAN (KEK) storage ring. The data are well described within the experimental uncertainties over the entire angular range.

JHEP09(2026)024

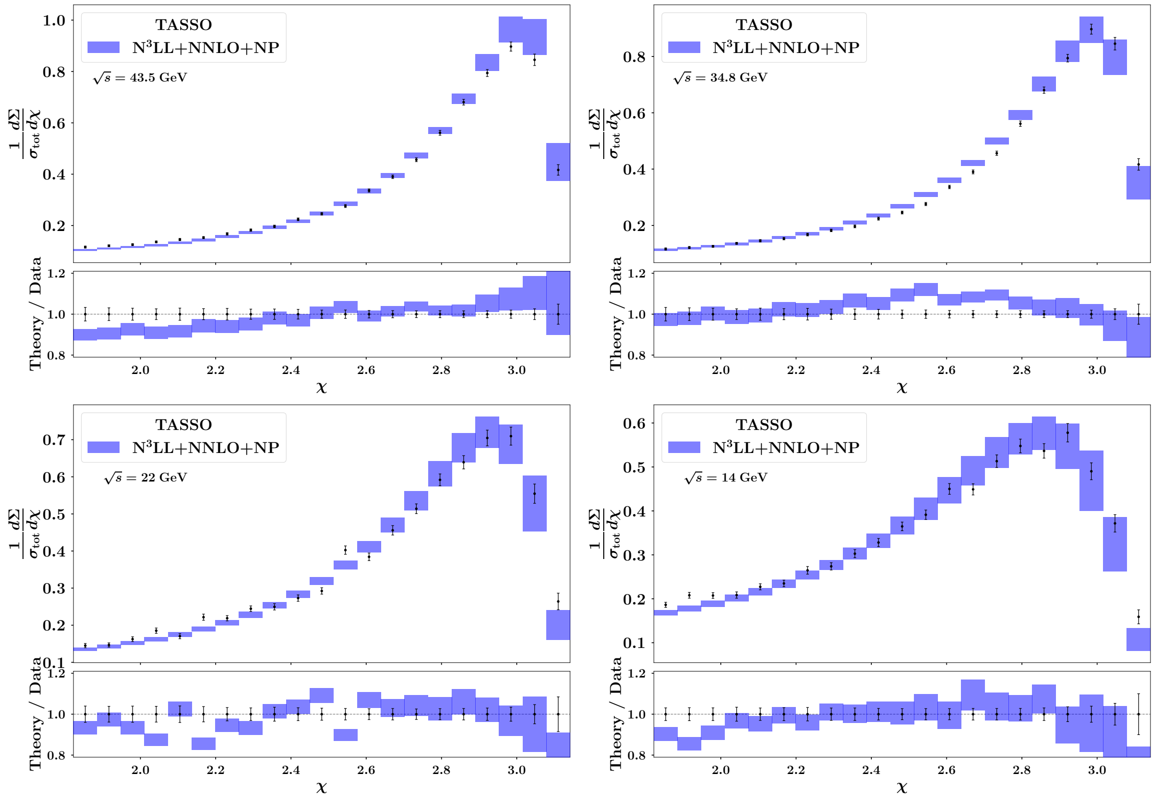

Figure 5. Comparison between experimental data and theoretical predictions (blue bands) for the EEC distribution from the TASSO Coll. at $\sqrt{s} = 43.5\,\text{GeV}$ (top left), $\sqrt{s} = 34.8\,\text{GeV}$ (top right), $\sqrt{s} = 22\,\text{GeV}$ (bottom left), and $\sqrt{s} = 14\,\text{GeV}$ (bottom right). The uncertainty bands represent the theoretical uncertainties estimated through scale variations. The lower panels show the ratio of the theoretical results to the experimental data.

In figures 5 and 6, we compare our predictions with data from the TASSO [47] and JADE [50] Collaborations at PETRA (DESY), and from the MAC Collaboration [53] at PEP (SLAC).

The shapes of the experimental distributions are well reproduced by our predictions, providing evidence that the adopted non-perturbative model is sufficiently flexible to describe data across a wide range of energies. As expected, the theoretical uncertainty bands increase at lower energies, reflecting the larger uncertainties associated with higher values of $\alpha_S(Q^2)$ and the relatively larger size of non-perturbative effects.

In figure 7 we compare our theoretical predictions with experimental data from the PLUTO Collaboration collected at DORIS II and PETRA (DESY), spanning nine center-of-mass energies from $\sqrt{s} = 34.6\,\text{GeV}$ down to $\sqrt{s} = 7.7\,\text{GeV}$. Despite the relatively large experimental uncertainties of these older datasets, our predictions provide a satisfactory description across the full energy range.

At $\sqrt{s} = 12\,\text{GeV}$ we are sufficiently above the Υ ($b\bar{b}$) resonances to safely neglect their effect. The highest Υ resonance has a mass $m \simeq 11\,\text{GeV}$ and a width $\Gamma \simeq 24\,\text{MeV}$.

At $\sqrt{s} = 9.4\,\text{GeV}$ we are quite close to the $\Upsilon(1S)$ resonance, which has a mass $m = 9460\,\text{MeV}$ and a width $\Gamma = 54.02\,\text{keV}$ (it is the lowest-lying vector resonance, with $J^{PC} = 1^{--}$,

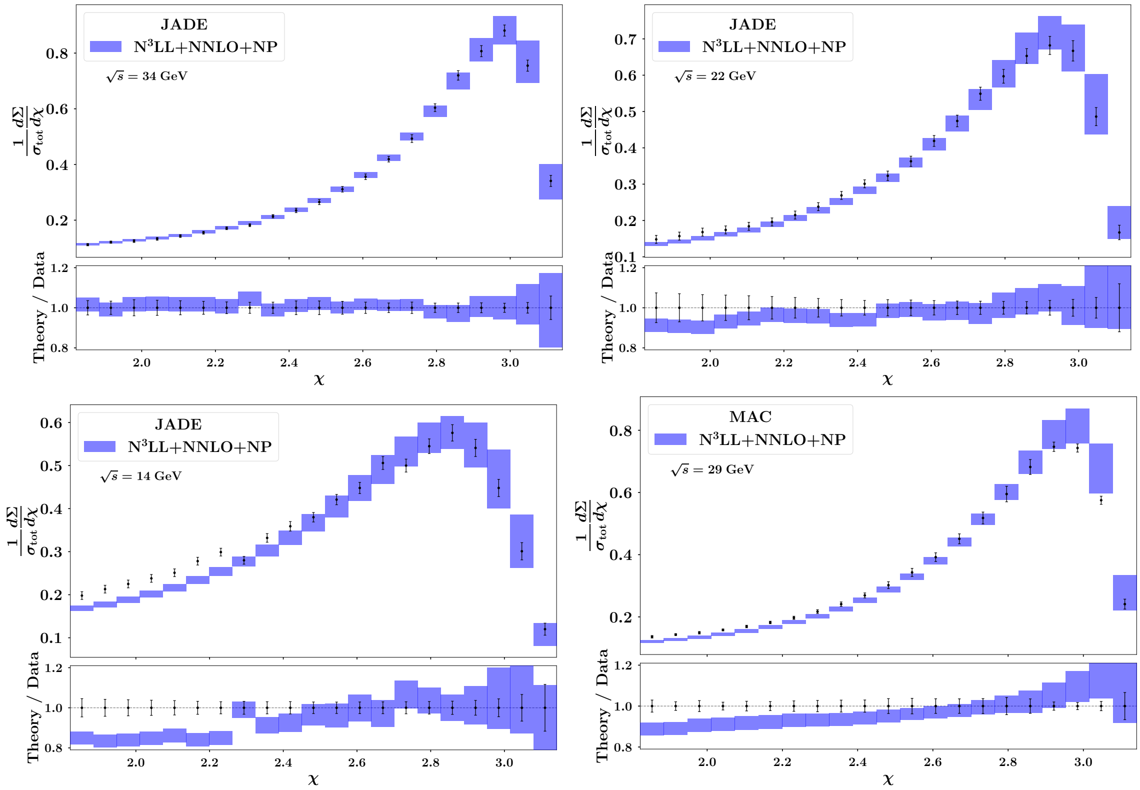

Figure 6. Comparison between experimental data and theoretical predictions (blue bands) for the EEC distribution from the JADE Coll. at $\sqrt{s} = 34, 22, 14\,\mathrm{GeV}$ (top left, top right, bottom left, respectively) and MAC Coll. at $\sqrt{s} = 29\,\mathrm{GeV}$ (bottom right). The uncertainty bands represent the theoretical uncertainties estimated through scale variations. The lower panels show the ratio of the theoretical results to the experimental data.

coupling to the time-like photon coming from e^+e^- annihilation). The dominant decay channel of this resonance is

$$\Upsilon(1S) \to 3g, \tag{4.3}$$

i.e. three (gluon) jets in the final state. In a more refined study of the EEC at this energy, one might try to estimate the impact of this resonance.

At $\sqrt{s} = 7.7\,\mathrm{GeV}$ we are below the bottom-quark threshold ($2m_b \sim 10\,\mathrm{GeV}$), so that the number of active flavours is $n_f = 4$. At this energy, charm-mass effects may be non-negligible, since

$$\frac{2m_c}{\sqrt{s}} \sim 0.4. \tag{4.4}$$

Their impact is enhanced by the electric charge of the charm quark,

$$\frac{Q_c^2}{Q_u^2 + Q_d^2 + Q_c^2 + Q_s^2} \simeq 0.4. \tag{4.5}$$

In figures 8 and 9 we compare our theoretical predictions with experimental data from the CELLO Collaboration at $\sqrt{s} = 34\,\mathrm{GeV}$ and $\sqrt{s} = 22\,\mathrm{GeV}$ collected at PETRA (DESY),

JHEP09(2026)024

$\alpha_S(m_Z^2)$	f_1 [GeV]	f_2 [GeV^2]	g_0
0.1192 ± 0.0028 $[0.0017_{\text{th.}} \pm 0.0015_{\text{exp.}} \pm 0.0016_{\text{corr.}}]$	1.0 ± 0.3	0.5 ± 0.3	0.9 ± 0.3

Table 2. Best-fit values and total uncertainties for $\alpha_S(m_Z^2)$ and the non-perturbative parameters.

and from the MARKII Collaboration at $\sqrt{s} = 29\,\text{GeV}$ (Run I and Run II) at PEP (SLAC), respectively. Although these datasets exhibit somewhat larger scatter with respect to the theoretical predictions compared to the higher-statistics measurements, an overall satisfactory description is achieved across the full angular range.

Table 2 lists the best-fit values and the associated uncertainties for the fitted parameters, namely $\alpha_S(m_Z^2)$ and the non-perturbative parameters entering eq. (2.15). Note that g_0 represents the non-perturbative component of the Collins-Soper evolution kernel $g_K(b)$ defined in eq. (2.17), while f_1 and f_2 characterize the non-perturbative function $f(b)$ defined in eq. (2.16).

The uncertainties are estimated following the procedure described in the previous section and correspond to the total uncertainty, including theoretical, experimental, and correlation-related contributions. In the case of $\alpha_S(m_Z^2)$, we separately indicate in square brackets the three individual contributions to the total uncertainty.

The extracted value of the strong coupling constant at the Z^0 scale, $\alpha_S(m_Z^2)$, is well constrained and consistent with the current PDG average [26]. The fitted non-perturbative parameters are also compatible with those obtained in previous analyses [21], which considered only data at the Z-boson mass. We observe that the inclusion of data at $Q < m_Z$ leads to a reduction of the uncertainties for all parameters, in particular for α_S.

In figure 10 we graphically represent the correlation matrix of the (free) fit parameters. In general, the absence of strong correlations or anti-correlations between all the parameters, which never exceed 0.21 in size, implies that their determination is not ambiguous. That is because the fit parameters play different roles in shaping the theoretical distribution. In particular, while f_1, f_2 and g_0 are related to power-like effects in the hard scale, α_S is related to logarithmic effects in Q.

The (small) anti-correlations of f_1 and f_2 with α_S both have the following origin. By increasing α_S, more radiation is emitted and the Sudakov form factor becomes broader, with its peak moving further away from the Born peak $\chi = \pi$. That implies that to reproduce again the data, smaller values of f_1 and f_2 are needed.

In order to further assess the impact of the ALEPH dataset on our results, and to provide an independent validation of our analysis, we have repeated the global fit excluding the ALEPH data entirely, retaining the remaining 610 data points obtaining a $\chi^2/N_{\text{d.o.f.}} = 1.25$. The extracted parameters are fully consistent with those of the baseline fit reported in table 2: we find $\alpha_S(m_Z^2) = 0.1189 \pm 0.0029$, with all non-perturbative parameters compatible within uncertainties with the values in table 2. The χ^2 per degree of freedom remains of order unity, confirming the stability and robustness of the fit with respect to the inclusion or exclusion of the ALEPH dataset. As a complementary check, we have also used the parameters extracted from the fit *without* ALEPH data to compute a theoretical prediction for the ALEPH dataset a posteriori (postdiction). The resulting description is excellent, with a χ^2 per degree of

JHEP09(2026)024

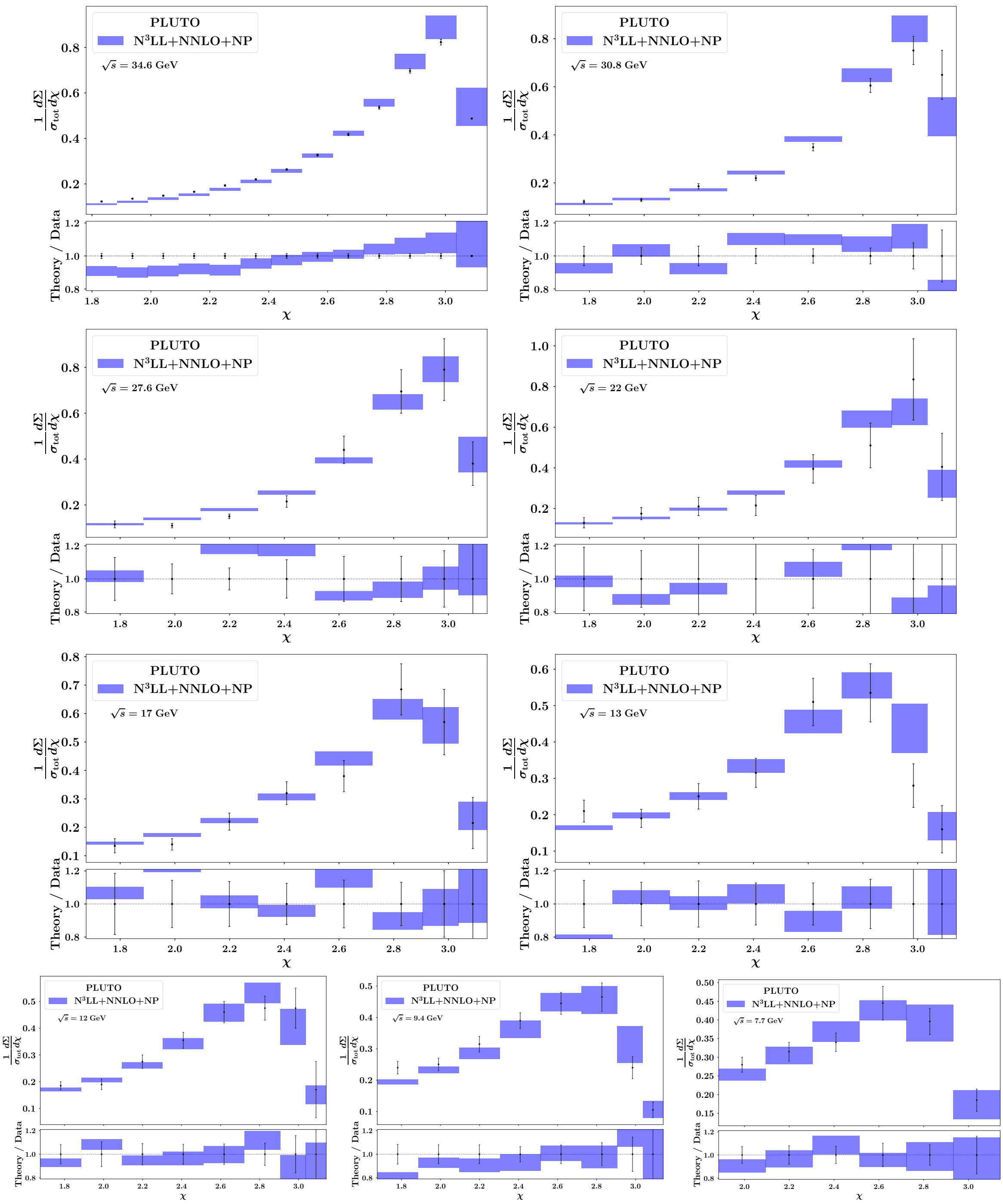

Figure 7. Comparison between experimental data and theoretical predictions (blue bands) for the EEC distribution from the PLUTO Coll. at $\sqrt{s} = 34.6, 30.8, 27.6, 22, 17, 13, 12, 9.4, 7.7$ GeV (from top left to bottom right). The uncertainty bands represent the theoretical uncertainties estimated through scale variations. The lower panels show the ratio of the theoretical results to the experimental data.

JHEP09(2026)024

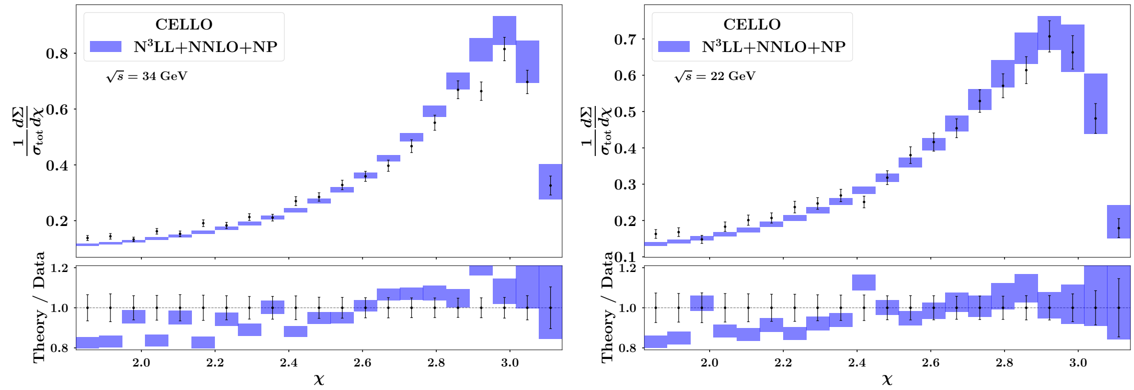

Figure 8. Comparison between experimental data and theoretical predictions (blue bands) for the EEC distribution from CELLO Coll. at $\sqrt{s} = 34\,\text{GeV}$ (left) and $\sqrt{s} = 22\,\text{GeV}$ (right). The uncertainty bands represent the theoretical uncertainties estimated through scale variations. The lower panels show the ratio of the theoretical results to the experimental data.

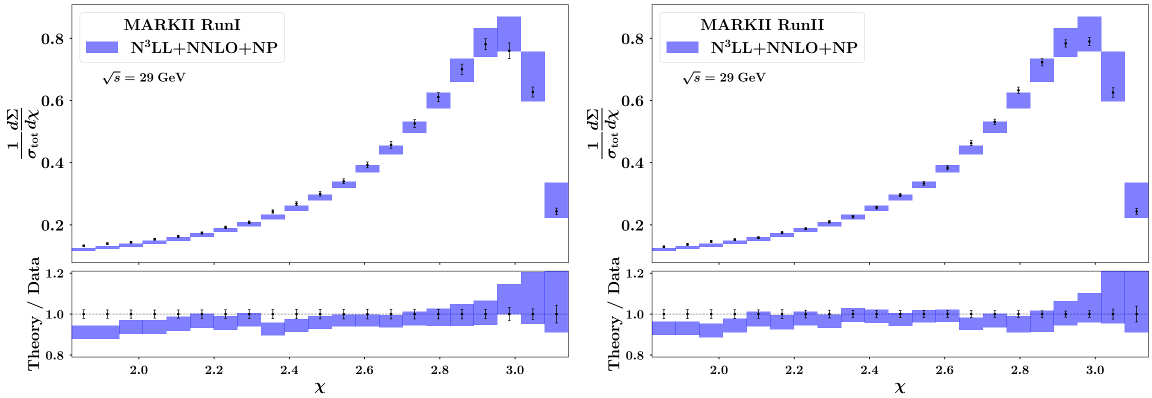

Figure 9. Comparison between experimental data and theoretical predictions (blue bands) for the EEC distribution from the MARKII Coll. for Run I (left) and Run II (right) at $\sqrt{s} = 29\,\text{GeV}$. The uncertainty bands represent the theoretical uncertainties estimated through scale variations. The lower panels show the ratio of the theoretical results to the experimental data.

freedom of order unity ($\chi^2/N_{\rm d.o.f.} = 1.02$), and no tension is observed between the theoretical prediction and the ALEPH measurements. Taken together, these results demonstrate that the ALEPH data are fully compatible with our theoretical framework and with the legacy datasets, and that their inclusion does not introduce any bias in the determination of α_S or the non-perturbative parameters. The ALEPH dataset should therefore be regarded as a high-precision independent confirmation of our analysis, rather than a source of systematic uncertainty.

We may therefore conclude that the (resummed) perturbative predictions for the inclusive and charged spectra are the same; in other words, the differences between the two spectra are non-perturbative in nature.

We emphasize that our study demonstrates that analytic dispersive models, such as the DMW model [25], can provide a consistent description of non-perturbative effects when supplemented by a term with explicit dependence on the hard scale Q, as also discussed in refs. [12, 13]. Indeed, as shown by several studies in the literature [8, 16, 21], and also

JHEP09(2026)024

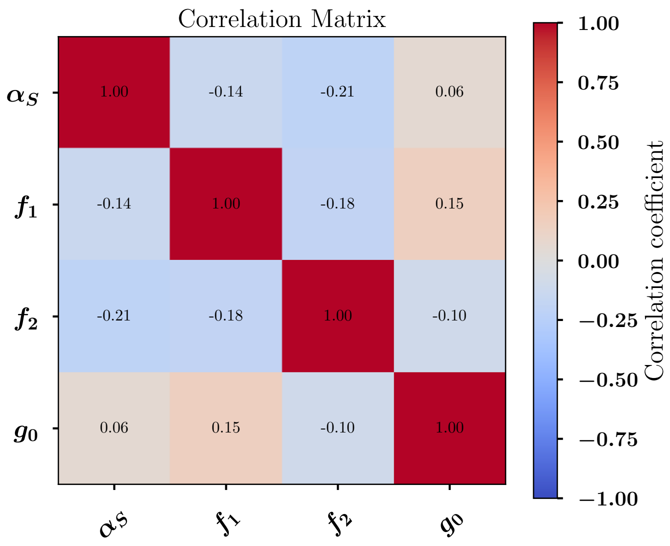

Figure 10. Graphical representation of the correlation matrix for the free fit parameters.

confirmed by the present analysis, an analytic NP model (without a Q-dependent contribution as Q is fixed) is capable of describing data at the Z-boson resonance with very good accuracy. In this work, we extend the analysis to data at different center-of-mass energies, finding a very good description of experimental measurements, once one additional non-perturbative parameter is added to model the Q-dependent evolution. In fact, as pointed out in ref. [17], without the inclusion of a Q-dependent non-perturbative term, it would not be possible to achieve a satisfactory description of the experimental data in a global fit. We have indeed checked that, by making independent fits for each center-of-mass energy, we obtain fitted values of the parameters f_2 which increase as the energy decreases. In other words, if we do remove the NP effects described by the function $g_K(b)$, and still fit data at different COM energies, in order to obtain a good description of the latter, we are forced to take f_2 dependent on the energy, i.e. $f_2 = f_2(Q)$.

In general, our results highlight the crucial role played by the Q-dependent non perturbative effects in the description of the observable across different center-of-mass energies.

In order to explore the potential impact of extending the available measurements to higher center-of-mass energies, we present in figure 11 our theoretical predictions for the EEC distribution at $\sqrt{s} = 133$, 172, and 206 GeV, corresponding to the energy range explored at CERN LEP2. Measurements at these energies would significantly extend the current kinematic coverage and provide a wider lever arm in Q. This would allow for a more stringent test of the predicted energy dependence of the observable and improve the determination of the non-perturbative contributions entering the resummed description.

4.1 Determination of the Collins-Soper evolution kernel

In recent years, the Collins-Soper kernel has received increasing attention due to its central role in the Transverse Momentum Distributions (TMD) framework, where it controls the evolution of TMDs with respect to the rapidity scale ζ [11, 32]. This interest is further motivated by

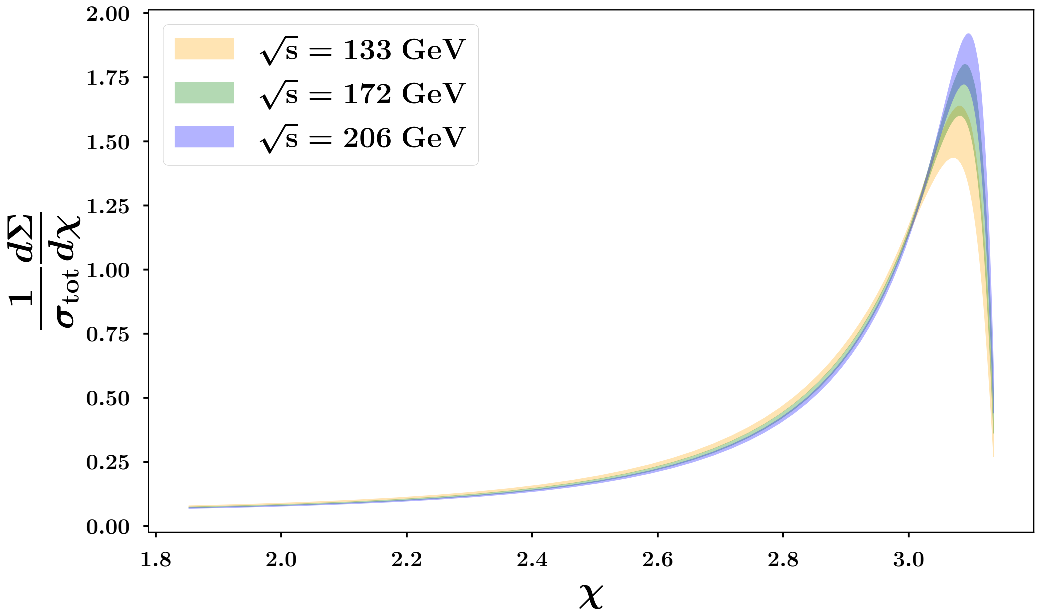

Figure 11. Theoretical predictions for the EEC distribution at $\sqrt{s} = 133$, 172, and 206 GeV.

the possibility of determining the kernel either from fits to experimental data [34, 54, 58–66], or theoretically through lattice QCD calculations [67–71].

Traditionally, the Collins-Soper evolution kernel has been extracted phenomenologically from Semi-Inclusive Deep Inelastic Scattering (SIDIS) [58, 62] and Drell-Yan (DY) data [34, 59–61, 63]. Extracting it from the EEC function [54, 64] in e^+e^- annihilation provides a highly complementary approach to the former. Since e^+e^- collisions are free from initial-state hadron effects, our extraction is entirely devoid of uncertainties related to Parton Distribution Functions (PDFs) and initial-state interactions, providing a uniquely clean environment to test the universality of the CS kernel.

The perturbative component of the Collins-Soper kernel satisfies the following RG evolution equation [31]:

$$\frac{dK\left[b^2Q^2, \alpha_S(Q^2)\right]}{d\ln Q^2} = -\gamma_K\left[\alpha_S(Q^2)\right], \tag{4.6}$$

where $\gamma_K(\alpha_S)$ denotes the cusp anomalous dimension. Solving this equation yields the following formula:

$$K\left[b^2Q^2, \alpha_S(Q^2)\right] = K\left[b_0^2, \alpha_S(b_0^2/b^2)\right] - \int_{b_0^2/b^2}^{Q^2} \frac{dq^2}{q^2}\gamma_K\left[\alpha_S(q^2)\right]. \tag{4.7}$$

The kernel can be perturbatively expanded as

$$K(b^2Q^2, \alpha_S) = \sum_{n=1}^{\infty}\left(\frac{\alpha_S}{\pi}\right)^n K^{(n)}(b^2Q^2). \tag{4.8}$$

As shown in ref. [31] and reported in ref. [34], the Collins-Soper kernel can be related, within our formalism, to the single and double-logarithmic resummation functions.

JHEP09(2026)024

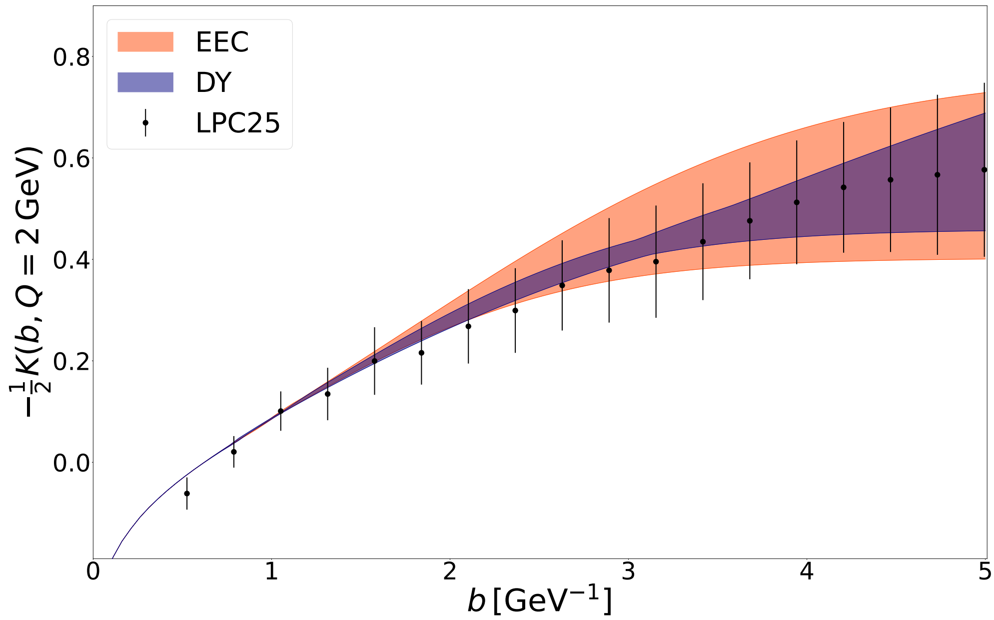

Figure 12. Collins-Soper kernel as a function of impact parameter b, at the scale $\mu_R = Q = 2\,\mathrm{GeV}$, extracted in this work (orange band) and compared with a determination from Drell-Yan data [34] (blue band) and with the most recent lattice result [71].

The NP component of the Collins-Soper evolution kernel is given by the energy dependent function $g_K(b)$ entering the NP Sudakov form factor in eq. (2.15). Thus, we have[3]

$$K(b, Q) = K(b_\star^2 Q^2, \alpha_S) - g_K(b)\,. \tag{4.9}$$

In figure 12 we present the Collins-Soper kernel as a function of the impact parameter b at the hard scale $Q = 2\,\mathrm{GeV}$, extracted from this analysis,[4] and we compare it with the determination obtained from a global study of Drell-Yan data at different energies [34], as well as with the most recent lattice QCD calculation [71]. As can be seen, the three determinations are in good mutual agreement for $b \lesssim 3\,\mathrm{GeV}^{-1}$, which corresponds to the region where both the perturbative expansion is reliable and the non-perturbative contributions are well constrained by the data. At higher values of b, the uncertainty bands broaden, as expected, given the reduced sensitivity of the kernel to the experimental data in this region. Nonetheless, the overall consistency between our EEC-based extraction, the Drell-Yan determination [34], and the most recent lattice QCD result [71], provides a non-trivial test of the universality of the Collins-Soper kernel in different processes and extraction methods.

In addition, we have performed a fit in which the value of g_0, i.e. the parameter controlling the size of the non-perturbative component of the Collins-Soper kernel, is kept fixed to the value obtained from the fit to Drell-Yan data of ref. [34]. In this case we obtain values of α_S and of the two remaining non-perturbative parameters that are fully compatible with those of our baseline extraction. This is consistent with what can be inferred from figure 10, which displays

[3]The plus sign in eq. (19) of ref. [34] is a typo; the correct sign is negative.

[4]To have a consistent estimation of the Collins-Soper kernel we perform different extractions by varying the value of $b_{\max}$ up to $2.5\,\mathrm{GeV}^{-1}$ as made also in ref. [34]. A similar study was made also in ref. [72].

only weak (anti-)correlations among the parameters: as discussed there, this is a consequence of the fact that they parameterize completely different non-perturbative behaviours.

4.2 Neglecting heavy-quark mass effects

The fitted values in table 2 have been obtained by including bottom-quark mass effects. In order to reach a general understanding of the form and the size of bottom-quark mass effects, we have repeated the fits by neglecting the bottom-quark mass, i.e. by setting $m_b = 0$. We find that the resulting theoretical predictions, the corresponding values of χ^2 and the extracted value of $\alpha_S(m_Z^2)$ with uncertainties, are comparable to those obtained by including the bottom-quark mass. However, the values of the fitted NP parameters are different:

$$f_1 : 1.0 \pm 0.3 \mapsto 0.7 \pm 0.3, \quad f_2 : 0.5 \pm 0.3 \mapsto 0.8 \pm 0.3, \quad g_0 : 0.9 \pm 0.3 \mapsto 1.1 \pm 0.4 \quad (m_b \mapsto 0).$$

That implies that perturbative mass effects can be effectively reabsorbed into a shift of the NP parameters. However, let us stress that the present analysis, involving bottom-quark mass effects, should be regarded as preliminary, since it still uses the massless hard factor and the massless remainder function (mass effects are included in the Sudakov form factor only). A more refined analysis, involving a wider χ range, and including *all* mass effects at $\mathcal{O}(\alpha_S)$, is left to future studies.

5 Conclusions

In this work, we have carried out a comprehensive global analysis of all available Energy-Energy Correlation (EEC) data in electron-positron annihilation, spanning center-of-mass energies from approximately 7.7 GeV up to 91.2 GeV, i.e. an energy span of over one order of magnitude. Our theoretical framework combines next-to-next-to-next-to-leading logarithmic (N^{3}LL) resummation in the back-to-back (two-jet) region with next-to-next-to-leading order (NNLO) fixed-order calculations, consistently matched over the full angular range. To compare our (partonic) calculations with experimental data, we have implemented a non-perturbative model incorporating energy-independent hadronization effects via an analytic dispersive approach, together with an explicit Q-dependent term. The latter turns out to be crucial for a unified description across different energies.

In our analysis, we perform the fit by consistently including data points from both the peak and intermediate regions in order to ensure a reliable extraction of the non-perturbative parameters and a solid determination of the strong coupling constant $\alpha_S(m_Z^2)$. The analysis achieves an excellent description of the complete dataset of 691 data points, with a $\chi^2/N_{\text{d.o.f.}} = 1.2$, validating both the theoretical framework and the chosen non-perturbative ansatz. As a primary result, we extracted a precise value of the strong coupling constant at the Z^0 scale, namely $\alpha_S(m_Z^2) = 0.1192 \pm 0.0028$ $[0.0017_{\text{th.}} \pm 0.0015_{\text{exp.}} \pm 0.0016_{\text{corr.}}]$, where the uncertainties quoted in square brackets indicate, respectively, the theoretical, the experimental uncertainties and the ones related to the correlation-models; the first is estimated through customary scale variations.

A key element of this work is the inclusion of the ALEPH and AMY datasets, which were incorporated into a global EEC fit for the first time. The excellent agreement found across the entire energy range, including these datasets, reinforces the consistency of our theoretical framework and the precision of the extracted value for the strong coupling constant, $\alpha_S(m_Z^2)$. Let us stress that including data over a wide range of center-of-mass energies is crucial, as it allows us to disentangle and determine the energy-dependent component of the non-perturbative model, which is directly related to the Collins-Soper evolution kernel. Thus, our analysis enables a novel and accurate extraction of this fundamental kernel from e^+e^- data.

We have also addressed the fact that the ALEPH dataset is based on charged final-state particles only. We have shown, both analytically and through dedicated PYTHIA simulations, that this affects the EEC only via an approximately shape-independent normalization factor, with negligible impact on the extracted value of $\alpha_S(m_Z^2)$ and of the non-perturbative parameters.

Finally, we present a preliminary investigation of heavy-quark (bottom-quark) mass effects. Including these effects does not significantly improve the quality of the fits, since that basically implies a shift of the non-perturbative parameters. In other words, once bottom-quark mass effects are included and theoretical spectra are refitted, one finds that the central values of the non-perturbative parameters are modified, while the related uncertainties are not. This fact implies that a first-principles (theoretical) determination of the non-perturbative parameters requires a full treatment of heavy quark mass effects, including also those ones entering the fixed-order distribution, which is a direction that represents a natural avenue for future work.

Acknowledgments

We would like to thank Gabor Somogyi for providing us with the numerical results of ref. [8], and Anthony Badea, Hannah Bossi, Francesco Hautmann and Stefan Kluth for useful discussions. We are also grateful to Dong Young Kim and the members of the AMY Collaboration for providing us the table with the EEC data of ref. [39].

The work of G.F. and L.R. is partially supported by the Italian Minister of University and Research (MUR) through the research grant 20229KEFAM (PRIN2022, Next Generation EU, CUP H53D23000980006).

Data Availability Statement. This article has no associated data or the data will not be deposited.

Code Availability Statement. This article has no associated code or the code will not be deposited.

References

[1] C.L. Basham, L.S. Brown, S.D. Ellis and S.T. Love, *Energy Correlations in electron-Positron Annihilation in Quantum Chromodynamics: Asymptotically Free Perturbation Theory*, *Phys. Rev. D* **19** (1979) 2018 [INSPIRE].

[2] C.L. Basham, L.S. Brown, S.D. Ellis and S.T. Love, *Energy Correlations in electron-positron Annihilation: Testing QCD*, *Phys. Rev. Lett.* **41** (1978) 1585 [INSPIRE].

[3] I. Moult and H.X. Zhu, *Energy Correlators: A Journey From Theory to Experiment*, arXiv:2506.09119 [INSPIRE].

[4] D.G. Richards, W.J. Stirling and S.D. Ellis, *Second Order Corrections to the Energy-energy Correlation Function in Quantum Chromodynamics*, *Phys. Lett. B* **119** (1982) 193 [INSPIRE].

[5] D.G. Richards, W.J. Stirling and S.D. Ellis, *Energy-energy Correlations to Second Order in Quantum Chromodynamics*, *Nucl. Phys. B* **229** (1983) 317 [INSPIRE].

[6] Z. Kunszt, P. Nason, G. Marchesini and B.R. Webber, *QCD at LEP*, in the proceedings of the *LEP Physics Workshop*, (1989) DOI:10.5170/CERN-1989-008-V-1.373 [INSPIRE].

[7] L.J. Dixon et al., *Analytical Computation of Energy-Energy Correlation at Next-to-Leading Order in QCD*, *Phys. Rev. Lett.* **120** (2018) 102001 [arXiv:1801.03219] [INSPIRE].

[8] Z. Tulipánt, A. Kardos and G. Somogyi, *Energy-energy correlation in electron-positron annihilation at NNLL + NNLO accuracy*, *Eur. Phys. J. C* **77** (2017) 749 [arXiv:1708.04093] [INSPIRE].

[9] V. Del Duca et al., *Three-Jet Production in Electron-Positron Collisions at Next-to-Next-to-Leading Order Accuracy*, *Phys. Rev. Lett.* **117** (2016) 152004 [arXiv:1603.08927] [INSPIRE].

[10] V. Del Duca et al., *Jet production in the CoLoRFulNNLO method: event shapes in electron-positron collisions*, *Phys. Rev. D* **94** (2016) 074019 [arXiv:1606.03453] [INSPIRE].

[11] J.C. Collins and D.E. Soper, *Back-To-Back Jets in QCD*, *Nucl. Phys. B* **193** (1981) 381 [*Erratum ibid.* **213** (1983) 545] [INSPIRE].

[12] J.C. Collins and D.E. Soper, *Back-To-Back Jets: Fourier Transform from B to K-Transverse*, *Nucl. Phys. B* **197** (1982) 446 [INSPIRE].

[13] J.C. Collins and D.E. Soper, *The Two Particle Inclusive Cross-section in e^+e^- Annihilation at PETRA, PEP and LEP Energies*, *Nucl. Phys. B* **284** (1987) 253 [INSPIRE].

[14] J. Kodaira and L. Trentadue, *Summing Soft Emission in QCD*, *Phys. Lett. B* **112** (1982) 66 [INSPIRE].

[15] J. Kodaira and L. Trentadue, *Single Logarithm Effects in electron-Positron Annihilation*, *Phys. Lett. B* **123** (1983) 335 [INSPIRE].

[16] D. de Florian and M. Grazzini, *The Back-to-back region in e^+e^- energy-energy correlation*, *Nucl. Phys. B* **704** (2005) 387 [hep-ph/0407241] [INSPIRE].

[17] A. Kardos et al., *Precise determination of $\alpha_S(M_Z)$ from a global fit of energy-energy correlation to NNLO+NNLL predictions*, *Eur. Phys. J. C* **78** (2018) 498 [arXiv:1804.09146] [INSPIRE].

[18] I. Moult and H.X. Zhu, *Simplicity from Recoil: The Three-Loop Soft Function and Factorization for the Energy-Energy Correlation*, *JHEP* **08** (2018) 160 [arXiv:1801.02627] [INSPIRE].

[19] M.A. Ebert, B. Mistlberger and G. Vita, *The Energy-Energy Correlation in the back-to-back limit at N^3LO and N^3LL'*, *JHEP* **08** (2021) 022 [arXiv:2012.07859] [INSPIRE].

[20] M. Jaarsma et al., *From DGLAP to Sudakov: Precision Predictions for Energy-Energy Correlators*, arXiv:2512.11950 [INSPIRE].

[21] U.G. Aglietti and G. Ferrera, *Energy-energy correlation in the back-to-back region at N3LL+NNLO in QCD*, *Phys. Rev. D* **110** (2024) 114004 [arXiv:2403.04077] [INSPIRE].

[22] R. Fiore, A. Quartarolo and L. Trentadue, *Energy-energy correlation for Theta → 180-degrees at LEP*, *Phys. Lett. B* **294** (1992) 431 [INSPIRE].

JHEP09(2026)024

[23] P. Nason and M.H. Seymour, *Infrared renormalons and power suppressed effects in e^+e^- jet events*, Nucl. Phys. B **454** (1995) 291 [hep-ph/9506317] [INSPIRE].

[24] Y.L. Dokshitzer, G. Marchesini and B.R. Webber, *Dispersive approach to power behaved contributions in QCD hard processes*, Nucl. Phys. B **469** (1996) 93 [hep-ph/9512336] [INSPIRE].

[25] Y.L. Dokshitzer, G. Marchesini and B.R. Webber, *Nonperturbative effects in the energy energy correlation*, JHEP **07** (1999) 012 [hep-ph/9905339] [INSPIRE].

[26] Particle Data Group collaboration, *Review of particle physics*, Phys. Rev. D **110** (2024) 030001 [INSPIRE].

[27] Electron-Positron Alliance collaboration, *Analysis note: measurement of energy-energy correlator in e^+e^- collisions at* 91 *GeV with archived ALEPH data*, arXiv:2505.11828 [INSPIRE].

[28] Electron-Positron Alliance collaboration, *Energy Correlators from Partons to Hadrons: Unveiling the Dynamics of the Strong Interactions with Archival ALEPH Data*, arXiv:2511.00149 [INSPIRE].

[29] G. Bozzi, S. Catani, D. de Florian and M. Grazzini, *Transverse-momentum resummation and the spectrum of the Higgs boson at the LHC*, Nucl. Phys. B **737** (2006) 73 [hep-ph/0508068] [INSPIRE].

[30] S. Catani, D. de Florian and M. Grazzini, *Universality of nonleading logarithmic contributions in transverse momentum distributions*, Nucl. Phys. B **596** (2001) 299 [hep-ph/0008184] [INSPIRE].

[31] J.C. Collins, D.E. Soper and G.F. Sterman, *Transverse Momentum Distribution in Drell-Yan Pair and W and Z Boson Production*, Nucl. Phys. B **250** (1985) 199 [INSPIRE].

[32] J. Collins, *Foundations of Perturbative QCD*, Cambridge University Press (2011) [DOI:10.1017/9781009401845] [INSPIRE].

[33] J. Collins and T. Rogers, *Understanding the large-distance behavior of transverse-momentum-dependent parton densities and the Collins-Soper evolution kernel*, Phys. Rev. D **91** (2015) 074020 [arXiv:1412.3820] [INSPIRE].

[34] S. Camarda, G. Ferrera and L. Rossi, *Drell-Yan lepton pair production at low invariant masses: transverse-momentum resummation and non-perturbative effects in QCD*, JHEP **01** (2026) 150 [arXiv:2508.06201] [INSPIRE].

[35] S. Camarda, G. Ferrera and M. Schott, *Determination of the strong-coupling constant from the Z-boson transverse-momentum distribution*, Eur. Phys. J. C **84** (2024) 39 [arXiv:2203.05394] [INSPIRE].

[36] ATLAS collaboration, *A precise determination of the strong-coupling constant from the recoil of Z bosons with the ATLAS experiment at $\sqrt{s} = 8$ TeV*, arXiv:2309.12986 [INSPIRE].

[37] U.G. Aglietti and G. Ferrera, *Heavy quark mass effects in the energy-energy correlation in the back-to-back region*, Eur. Phys. J. C **85** (2025) 272 [arXiv:2412.02629] [INSPIRE].

[38] R.K. Ellis, W.J. Stirling and B.R. Webber, *QCD and collider physics*, Cambridge University Press (2011) [DOI:10.1017/CBO9780511628788] [INSPIRE].

[39] AMY collaboration, *Measurement of α_s using NLLA + $O(\alpha_s^2)$ in e^+e^- annihilation at $\sqrt{s} = 58$-GeV*, Phys. Lett. B **420** (1998) 233 [INSPIRE].

[40] OPAL collaboration, *An improved measurement of α_s (M (Z0)) using energy correlations with the OPAL detector at LEP*, Phys. Lett. B **276** (1992) 547 [INSPIRE].

JHEP09(2026)024

[41] OPAL collaboration, *A determination of α_s (M (Z0)) at LEP using resummed QCD calculations*, Z. Phys. C **59** (1993) 1 [INSPIRE].

[42] DELPHI collaboration, *Determination of alpha(s) in second order QCD from hadronic Z decays*, Z. Phys. C **54** (1992) 55 [INSPIRE].

[43] DELPHI collaboration, *Determination of α_s using the next-to-leading log approximation of QCD*, Z. Phys. C **59** (1993) 21 [INSPIRE].

[44] L3 collaboration, *Determination of α_s from hadronic event shapes measured on the Z0 resonance*, Phys. Lett. B **284** (1992) 471 [INSPIRE].

[45] SLD collaboration, *Measurement of $\alpha_s(M_Z^2)$ from hadronic event observables at the Z0 resonance*, Phys. Rev. D **51** (1995) 962 [hep-ex/9501003] [INSPIRE].

[46] TOPAZ collaboration, *Measurements of α_s in e^+e^- Annihilation at $\sqrt{s} = 53.3$-GeV and 59.5-GeV*, Phys. Lett. B **227** (1989) 495 [INSPIRE].

[47] TASSO collaboration, *A Study of Energy-energy Correlations Between 12-GeV and 46.8-GeV CM Energies*, Z. Phys. C **36** (1987) 349 [INSPIRE].

[48] PLUTO collaboration, *A Study of Energy-energy Correlations in e^+e^- Annihilations at $\sqrt{s} = 34.6$-GeV*, Z. Phys. C **28** (1985) 365 [INSPIRE].

[49] PLUTO collaboration, *Energy-energy Correlations in e^+e^- Annihilation Into Hadrons*, Phys. Lett. B **99** (1981) 292 [INSPIRE].

[50] JADE collaboration, *Measurements of Energy Correlations in $e^+e^- \to$ Hadrons*, Z. Phys. C **25** (1984) 231 [INSPIRE].

[51] CELLO collaboration, *Analysis of the Energy Weighted Angular Correlations in Hadronic e^+e^- Annihilations at 22-GeV and 34-GeV*, Z. Phys. C **14** (1982) 95 [INSPIRE].

[52] D.R. Wood et al., *Determination of α_s From Energy-energy Correlations in e^+e^- Annihilation at 29-GeV*, Phys. Rev. D **37** (1988) 3091 [INSPIRE].

[53] E. Fernandez et al., *A Measurement of Energy-energy Correlations in $e^+e^- \to$ Hadrons at $\sqrt{s} = 29$-GeV*, Phys. Rev. D **31** (1985) 2724 [INSPIRE].

[54] A.B. Cuerpo, I. Scimemi and A. Vladimirov, *Assessing the sensitivity of energy-energy correlations in e^+e^- annihilation to TMD dynamics*, JHEP **11** (2025) 013 [arXiv:2507.17478] [INSPIRE].

[55] NNPDF collaboration, *A determination of parton distributions with faithful uncertainty estimation*, Nucl. Phys. B **809** (2009) 1 [*Erratum ibid.* **816** (2009) 293] [arXiv:0808.1231] [INSPIRE].

[56] R.D. Ball et al., *Parton Distribution Benchmarking with LHC Data*, JHEP **04** (2013) 125 [arXiv:1211.5142] [INSPIRE].

[57] C. Bierlich et al., *A comprehensive guide to the physics and usage of PYTHIA 8.3*, SciPost Phys. Codeb. **2022** (2022) 8 [arXiv:2203.11601] [INSPIRE].

[58] MAP (Multi-dimensional Analyses of Partonic distributions) collaboration, *Flavor dependence of unpolarized quark transverse momentum distributions from a global fit*, JHEP **08** (2024) 232 [arXiv:2405.13833] [INSPIRE].

[59] MAP (Multi-dimensional Analyses of Partonic distributions) collaboration, *Neural-Network Extraction of Unpolarized Transverse-Momentum-Dependent Distributions*, Phys. Rev. Lett. **135** (2025) 021904 [arXiv:2502.04166] [INSPIRE].

[60] F. Aslan et al., *Phenomenology of TMD parton distributions in Drell-Yan and Z0 boson production in a hadron structure oriented approach*, Phys. Rev. D **110** (2024) 074016 [arXiv:2401.14266] [INSPIRE].

[61] V. Moos, I. Scimemi, A. Vladimirov and P. Zurita, *Extraction of unpolarized transverse momentum distributions from the fit of Drell-Yan data at N^{4}LL*, JHEP **05** (2024) 036 [arXiv:2305.07473] [INSPIRE].

[62] V. Moos, I. Scimemi, A. Vladimirov and P. Zurita, *Determination of unpolarized TMD distributions from the fit of Drell-Yan and SIDIS data at N^{4}LL*, JHEP **11** (2025) 134 [arXiv:2503.11201] [INSPIRE].

[63] P.C. Barry et al., *First simultaneous analysis of transverse momentum dependent and collinear parton distributions in the proton*, arXiv:2510.13771 [INSPIRE].

[64] Z.-B. Kang, J. Penttala and C. Zhang, *Determination of the strong coupling constant and the Collins-Soper kernel from the energy-energy correlator in e^+e^- collisions*, arXiv:2410.21435 [INSPIRE].

[65] MAP (Multi-dimensional Analyses of Partonic distributions) collaboration, *Unpolarized transverse momentum distributions from a global fit of Drell-Yan and semi-inclusive deep-inelastic scattering data*, JHEP **10** (2022) 127 [arXiv:2206.07598] [INSPIRE].

[66] A. Avkhadiev et al., *Extraction of the Collins-Soper Kernel from a Joint Analysis of Experimental and Lattice Data*, Phys. Rev. Lett. **136** (2026) 171902 [arXiv:2510.26489] [INSPIRE].

[67] Lattice Parton (LPC) collaboration, *Lattice calculation of the intrinsic soft function and the Collins-Soper kernel*, JHEP **08** (2023) 172 [arXiv:2306.06488] [INSPIRE].

[68] A. Avkhadiev, P.E. Shanahan, M.L. Wagman and Y. Zhao, *Determination of the Collins-Soper Kernel from Lattice QCD*, Phys. Rev. Lett. **132** (2024) 231901 [arXiv:2402.06725] [INSPIRE].

[69] D. Bollweg, X. Gao, S. Mukherjee and Y. Zhao, *Nonperturbative Collins-Soper kernel from chiral quarks with physical masses*, Phys. Lett. B **852** (2024) 138617 [arXiv:2403.00664] [INSPIRE].

[70] D. Bollweg et al., *Transverse-momentum-dependent pion structures from lattice QCD: Collins-Soper kernel, soft factor, TMDWF, and TMDPDF*, Phys. Rev. D **112** (2025) 034501 [arXiv:2504.04625] [INSPIRE].

[71] J.-X. Tan et al., *Lattice QCD determination of the Collins-Soper kernel in the continuum and physical mass limits*, Phys. Rev. D **113** (2026) 054505 [arXiv:2511.22547] [INSPIRE].

[72] M. Cerutti and A. Simonelli, *The impact of prescriptions in phenomenological extractions of transverse momentum dependent distributions*, Eur. Phys. J. C **86** (2026) 956 [arXiv:2603.19088] [INSPIRE].